

Quantum and classical glasses of ultrasoft particles in two dimensions

Rogelio Díaz-Méndez,¹ Fabio Mezzacapo,¹ Fabio Cinti,² Wolfgang Lechner,³ and Guido Pupillo¹

¹IPCMS (UMR 7504) and ISIS (UMR 7006), Université de Strasbourg and CNRS, Strasbourg, France

²National Institute for Theoretical Physics (NITheP), Stellenbosch 7600, South Africa

³IQOQI and Institute for Theoretical Physics, University of Innsbruck, Austria

(Dated: December 3, 2024)

We study the phases and dynamics of monodisperse particles interacting via soft-core potentials in two spatial dimensions of interest for soft-matter colloidal systems and quantum atomic gases. Using exact theoretical methods, we demonstrate that the equilibrium low-temperature classical phase simultaneously breaks both translational symmetry and dynamic space-time homogeneity, usually associated with out-of-equilibrium glassy phenomena. This results in an exotic self-assembled cluster crystal with coexisting liquid-like dynamical properties, such as linear diffusion with time. The dynamics following a temperature quench into this phase leads to a monodisperse glass. We find that quantum fluctuations and bosonic statistics can have opposite effects: the former tend to destabilize the crystal into a liquid, while the latter can result in a surprising opposite effect.

PACS numbers: 64.70.P-, 67.10.Fj, 32.80.Ee

The discovery of novel phases of matter as a result of broken symmetries is of main interest in condensed matter. In quantum physics, a key example is the supersolid phase for bosonic particles [1–3], where the rare simultaneous breaking of two symmetries (i.e., continuous translational and global gauge symmetry) leads to the coexistence of both crystalline and superfluid properties [4–10]. A phase that does not fall into this scheme is the glass phase, both classical and quantum, which is a non-equilibrium and disordered - yet stable - phase [11, 12]. In analogy to the picture of broken symmetries, however, the glass transition is often associated with breaking of space-time homogeneity, or *dynamic heterogeneity*. The latter is a result of frustration effects, known as self-caging [13], and corresponds to a relaxation that is fast on a local scale, and exponentially slow on large-ones [14–20]. The search for novel mechanisms for caging and glass effects both in the classical [21] and quantum [22–25] regimes is of central interest in condensed matter, as well as atomic and molecular physics [26, 27].

In this work we analyse numerically the classical to quantum transition of non-equilibrium and equilibrium phases in a model system of ultra-soft particles, finding several novel features. We demonstrate theoretically that (i) the equilibrium phase is an exotic ordered cluster crystal with a dynamical separation between intra-cluster particle motion and hopping, inducing dynamic heterogeneity *at equilibrium*. This is microscopically due to caging effects at the level of individual clusters, which result in the coexistence of crystalline and liquid-like properties, such as linear particle diffusion as a function of time t . This is a classical version of a supersolid thermodynamic phase. (ii) The non-equilibrium phase after a quench can be disordered and display glass-like properties. This is surprising, since, unlike regular glass-forming liquids, where frustration stems from polydispersity of the ensemble, anisotropy of interactions, or the competition between interactions and geometry of substrates,

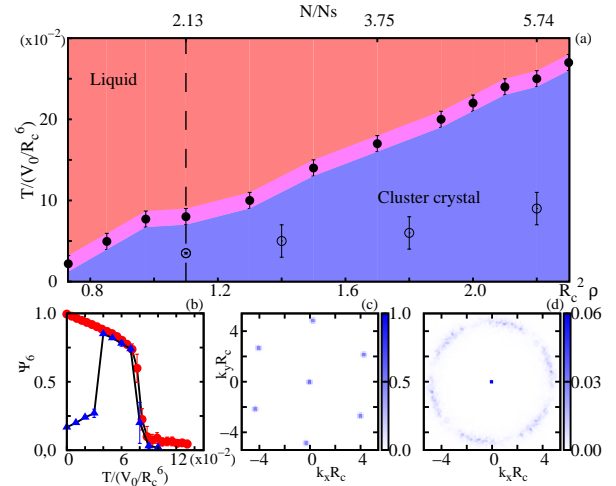


FIG. 1: (color online) (a) Phase diagram as a function of scaled temperature $T/(V_0/R_c^6)$ and density $R_c^2\rho$ for classical monodisperse particles with soft-core interactions [see Eq. (1)] at equilibrium. N/N_s is the average number of particles per cluster in the ground-state [upper x -axis]. Dashed line: $R_c^2\rho \simeq 1.1$ [see panel (b)]. Empty dots signal the glass transition temperature T_g after a quench. (b) Cluster short-range orientational order Ψ_6 as a function of T at equilibrium (circles) and after a quench (triangles), for $R_c^2\rho \simeq 1.1$ [dashed line in panel (a)]. Static structure factor for $R_c^2\rho \simeq 1.1$ and $T/(V_0/R_c^6) = 0.02$ at equilibrium (c) and after quench (d).

here the gas is monodisperse, the interactions isotropic, and geometric frustration is inhibited by the low spatial dimension [21]. Equally important, (iii) we use a combination of numerically exact semiclassical and fully quantum techniques to elucidate the different effects of quantum fluctuations and quantum statistics on the novel phenomena described here. Surprisingly, we find that these are competing: zero-point motion tends to destabilize the cluster crystal in favor of liquid-like phases, while bosonic quantum statistics can have the opposite effect

of enhancing crystalline behavior. These effects are at odds with results for polydispersed hard spheres [22, 28], where large quantum fluctuations appear to help crystallization, and systems such as He⁴ or dipolar crystals [25], where bosonic statistics always favors a liquid behavior, respectively. Some of these effects may be relevant for systems as diverse as colloidal particles [21, 29, 30] as well as cold gases of Rydberg dressed atoms [31, 32].

We consider a two-dimensional ensemble of N bosonic particles with mass m , density ρ and Hamiltonian

$$\hat{H} = -\frac{\hbar^2}{2m} \sum_{i=1}^N \nabla_i^2 + \sum_{i<j}^N \frac{V_0}{r_{ij}^\gamma + R_c^\gamma}. \quad (1)$$

The interaction in Eq. (1) approaches a constant value V_0/R_c^γ as the inter-particle distance, r , decreases below the soft-core distance R_c , and drops to zero for $r > R_c$. The case $\gamma \rightarrow \infty$ yields the soft-disc model [33]. Here we focus on $\gamma = 6$, corresponding to soft-core van der Waals interactions of relevance for ultracold atoms [6, 34].

Particles with soft-core interactions have been studied previously [35–38] in the classical high-temperature regime ($\hbar = 0, T \neq 0$), and in the purely quantum zero-temperature regime ($\hbar \neq 0, T = 0$) [6–8]. In the former case, it has been shown that pair potentials with a negative Fourier component [35] favor the formation of particle clusters, which in turn can crystallize to form so-called classical cluster-crystals. In the latter case, bosonic quantum statistics can turn the cluster-solid into a supersolid phase via a quantum phase transition at a critical value $\alpha_{cs-ss} \simeq 40$ where $\rho m V_0 / (\hbar^2 R_c^2) \equiv \alpha$ [8]. The supersolid further melts into a superfluid phase via a first order quantum phase transition at $\alpha_{ss-sf} \simeq 30$. Here, we bridge the gap between the classical and quantum regimes by first analyzing the static and dynamic properties in the classical regime, and then studying the separate effects of quantum fluctuations and statistics.

Equilibrium phase diagram -. In the classical case ($\hbar = 0, T \neq 0$), results are obtained at thermodynamic equilibrium by means of careful annealing, using Langevin molecular dynamics simulations [39]. The various phases are obtained by computing both static and dynamic physical observables in a wide range of T and ρ for systems of up to $N = 3120$. The resulting phase diagram is shown in Fig. 1(a) as a function of $T/(V_0/R_c^6)$ and the rescaled density $R_c^2 \rho \gtrsim 1$. At low T we find an ordered crystalline phase consisting of clusters arranged in a triangular configuration [see, e.g., snapshot in Fig. 3(a)], each cluster comprising an average number of particles larger than one and increasing with $R_c^2 \rho$. The static structure factor $S(\mathbf{k}) = \langle |\sum_j^N e^{i\mathbf{k}\cdot\mathbf{r}_j}|^2 / N \rangle$ measuring long-range positional order displays well defined peaks in this ordered phase [Fig. 1(c)]. Here, \mathbf{k} is a wave vector, \mathbf{r}_j the position of the j -th particle, and $\langle \dots \rangle$ denotes averaging over many configurations. For high T , instead, we find a normal liquid phase with no peaks in

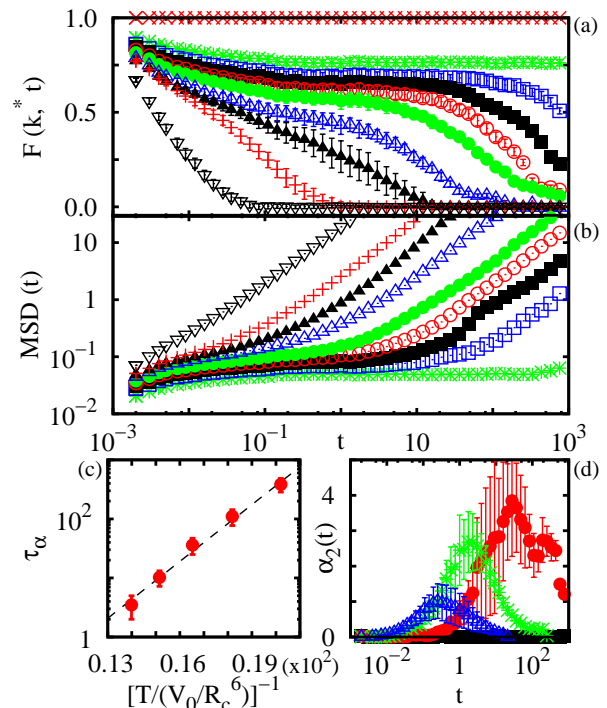


FIG. 2: (color online) (a) self-intermediate scatter function $F(k^*, t)$ vs. computational time t for $T/(V_0/R_c^6) \times 10^2 = 0, 3.3, 4.4, 4.95, 5.5, 6.05, 7.15, 7.70, 8.25,$ and 13.2 (top to bottom). (b): mean square displacement (in units of R_c^2) $MSD(t)$ vs. t ; symbols are the same as above. (c): relaxation time τ_α defined via $F(k^*, \tau_\alpha) = e^{-1}$. The dashed line is an exponential fitting function (see text). (d): non-gaussian parameter $\alpha_2(t)$ vs. t for $T/(V_0/R_c^6) = 0.03$ (squares), 0.05 (circles), 0.07 (stars), 0.08 (triangles). Data refer scaled density $R_c^2 \rho = 1.1$.

$S(\mathbf{k})$ for $\mathbf{k} \neq 0$ independently of $R_c^2 \rho$, as expected.

We characterize quantitatively the finite- T melting transition between these two phases by monitoring the hexatic (short-range) bond-order parameter of the clusters, which we define as $\Psi_6 = \langle |\sum_j^{N_c} \sum_l^{N_j} e^{i6\theta_{jl}} / (N_c N_j)| \rangle$ in analogy to regular non-cluster forming crystals (see [40] for details and [42]). Here N_c is the total number of clusters, N_j is the number of clusters neighboring the j -th one, and θ_{jl} is the angle between a reference axis and the segment joining the clusters j and l . The parameter $\Psi_6(T)$ decreases from $\Psi_6 = 1$ at $T = 0$ to $\Psi_6 \simeq 0$ in the liquid phase. The observed jump at the transition point is system size independent for $N_c \gtrsim 200$ and consistent with a first order transition [see red dots in Fig. 1(b) for an example]. We find that for $R_c^2 \rho \gtrsim 1$ the classical melting temperature T_M grows essentially linearly with $R_c^2 \rho$, with a scaling of the critical interaction strength $\alpha_{cc-l} \equiv \rho V_0 / (T_M R_c^4) \simeq 0.16$.

The dynamics of the equilibrium phases of Fig. 1 is initially characterized by computing the mean square displacement $MSD(t) = \langle \Delta r^2(t) \rangle = \langle \sum_j |\mathbf{r}_j(0) - \mathbf{r}_j(t)|^2 / N \rangle$ as well as the time-dependent self-intermediate scatter function $F(k^*, t) = \langle \sum_j e^{i\mathbf{k}^* \cdot [\mathbf{r}_j(0) - \mathbf{r}_j(t)]} / N \rangle$, where $k^* =$

$|\mathbf{k}^*|$ refers to the characteristic momentum of the main peak in $S(\mathbf{k})$ [26]. The latter quantities provide complementary information on particle mobility and time-correlations of particle positions within the crystal, respectively [43]: For example, in the liquid phase, $MSD(t)$ follows the usual linear diffusion law $MSD(t) \propto t$ [44] typical for Brownian motion, while $F(k^*, t)$ decays exponentially. For non-cluster-forming crystals, both quantities are essentially constant (see [42] for pure power-law interactions $\sim 1/r^6$ in 2D).

For model Eq. (1) the situation is however strikingly different. For $T \lesssim T_M$ the time evolution of both observables interpolates between the solid and liquid regimes: an extended plateau is followed by linear diffusion for $MSD(t)$ and exponential decay for $F(k^*, t)$, respectively, the size of the plateaus increasing with decreasing T . An analysis of the T -dependent relaxation time τ_α for which $F(k^*, \tau_\alpha) = 1/e$ reveals an Arrhenius-type exponential dependence on $1/T$ without detectable saturation [see, e.g., Fig. 2(c)], indicating that the liquid-like diffusion described here is thermally activated, and only vanishes at $T = 0$. By inspection of particle configurations, we determine that the microscopic diffusion mechanism here corresponds to hopping of particles between different clusters (see snapshots in Fig. S2 of [42]), leaving the underlying crystal structure essentially unaltered. These behaviors indicate the existence of *liquid-like particle diffusion within the crystalline phase at equilibrium*.

We find that to the emergence of liquid properties within the crystal corresponds the appearance of so-called *dynamic heterogeneity*. The latter corresponds to the presence of spatial correlations in the *dynamics* [11, 12], indicating a coexistence between space-time regions where particle motion is abundant and regions where motion is rare. This is demonstrated for our model in Fig. 2(d) by a peak in the non-gaussian parameter $\alpha_2 = [\langle \Delta r^4(t) \rangle / 2 \langle \Delta r^2(t) \rangle^2] - 1$, [13, 45]. The latter measures deviations from gaussian fluctuations in the distributions of displacements, and thus is in general $\alpha_2(t) = 0$ for all t in regular liquids and non-cluster crystals at equilibrium. Here, however, for $T < T_M$ and intermediate times we obtain $\alpha_2(t) \neq 0$, since the particles can be differentiated in *fast* and *slow* due to deconfined inter-cluster hopping and confined intra-cluster motion.

We note that the phenomenology of the dynamics described above [e.g., dynamical heterogeneity, two-step behavior of MDS and $F(k^*, \tau_\alpha)$] is usually associated with glass-forming liquids out-of-equilibrium. The demonstration of the existence of a novel thermodynamic classical phase with coexisting structural order and liquid-like properties is, to our knowledge, a prime, and constitutes one of the central results of this work. We notice that this phase constitutes a classical counterpart of a recently discovered cluster supersolid in the quantum regime, where a crystal coexists with superfluidity.

A monodisperse isotropic glass - . Quenching temper-

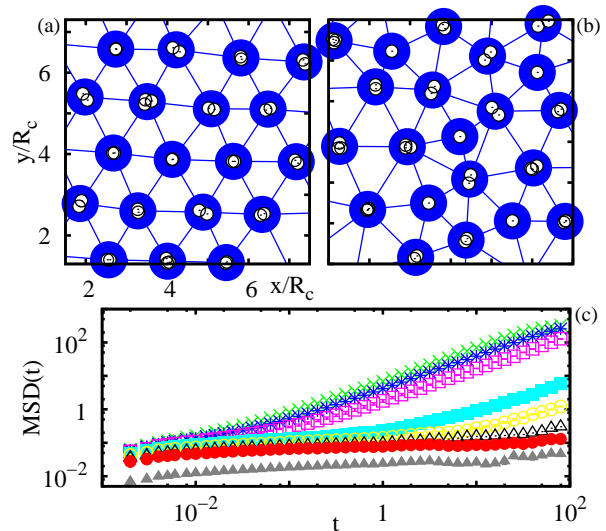


FIG. 3: (color online) Snapshots at equilibrium (a) and after a quench (b) of part of the system for $T/(V_0/R_c^6) = 0.02$ and $R_c^2\rho \simeq 1.1$. Full (empty) symbols represent clusters (individual particles). Lines connect neighboring clusters. (c) MSD vs t (in units of R_c^2) after quench. Data refer to $R_c^2\rho \simeq 1.1$ and $T/(V_0/R_c^6) \times 10^2 = 10, 9, 8, 7, 6, 5, 4, 1$ (top to bottom).

ature from an initial $T \gg T_M$ to a final $T < T_g < T_M$ causes the disappearance of structural order and the realization of a *glassy phase* below a glass transition temperature T_g . This is exemplified in Fig. 2(d), where $S(\mathbf{k})$ computed after a given long waiting time $t^* = 10^2$ following a quench to $T < T_g$ presents a very weak ring-like structure characteristic of non-crystalline systems [here $T_g/(V_0/R_c^6) \approx 0.04$]: In the glassy phase clusters do not form a regular structure [Fig. 3(b)], as the system is frustrated by, e.g., large fluctuations in the numbers of particles per cluster and number of nearest neighbor clusters. This is in stark contrast to the equilibrium case above.

The transition temperature T_g is usually obtained by monitoring dynamic properties, such as $MSD(t)$. The latter develops a characteristic plateau for $T \lesssim T_g$ [Fig. 3(c)], usually associated to “caging effects”: close to a glass transition, mobility of individual particles is increasingly limited by interactions with their neighbors. This is different from the equilibrium case above, where the long-time dynamics is liquid-like for any $T > 0$ [i.e., linear diffusion in $MSD(t)$ for long t].

We find that the glass transition temperature T_g can be also directly obtained by computing the time-independent parameter $\Psi_6(T)$: While for $T_g < T < T_M$ the values of Ψ_6 are essentially indistinguishable from their equilibrium counterpart [Fig. 1(b), blue triangles], signaling a finite equilibration time, for $T < T_g$ we observe loss of ergodicity and consequent lack of equilibration with $\Psi_6 \ll 1$. The change of behavior is abrupt around T_g and results in the absence of crystal formation, which is captured by a jump in $\Psi_6(T)$. We find that

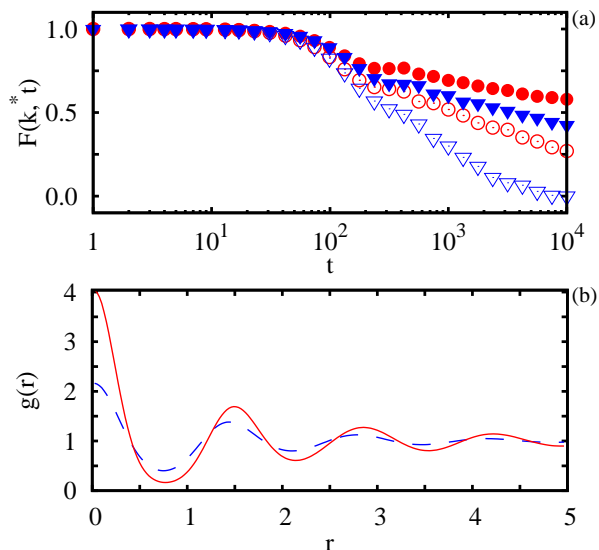


FIG. 4: (color online) (a): $F(k^*, t)$ computed by Path Integral Langevin Dynamics. Data are for $R_c^2\rho = 0.8119$, $mV_0/(\hbar^2 R_c^4) = 80$ (circles) and 60 (triangles). T values are 1.6 and 2.6 (full and open symbols, respectively), in units of $\hbar^2/(mR_c^2)$. (b): $g(r)$ computed via Path Integral Monte Carlo simulations with and without bosonic quantum exchanges (solid and dashed line, respectively). Here $T/[\hbar^2/(mR_c^2)] = 10$, $mV_0/(\hbar^2 R_c^4) = 35$, and $R_c^2\rho = 2.029$.

the estimate for T_g from $\Psi_6(T)$ is in agreement with that extracted from $MSD(t)$ above. This may make the observation of the glass transition possible in, e.g., Rydberg systems, where effects such as, e.g., spontaneous emission may hinder the monitoring of the long-time dynamics.

The existence of a glass phase in our model Eq. (1) constitutes the second main result of this work. Its occurrence is surprising, since glasses are usually favored by frustration induced by polydispersity, interaction anisotropy, or geometry in higher dimensions. Results consistent with those presented here have been recently discussed for mixtures of three-dimensional glass-forming classical colloidal dendrimers in [46].

Quantum effects ($\hbar \neq 0$, $T > 0$) on the phase diagram of Fig. 1 are investigated numerically in the semiclassical approximation using Path Integral Langevin Dynamics (PIMD) [28] and fully quantum mechanically using exact quantum Path Integral Monte Carlo methods (PIMC) [47]. These provide complementary information: PIMD neglects particle exchange and the classical limit is the real-time dynamics of the particles, while PIMC treats the bosonic statistics exactly in imaginary time.

Figure 4(a) shows results for $F(k^*, t)$ defined above using PIMD. We choose here scaled densities such as $\alpha \gtrsim \alpha_{cs-ss}$, so that the zero-temperature quantum phase is a cluster crystal. In full generality, Fig. 4(a) shows that semiclassical quantum fluctuations (e.g., "zero-point motion") cooperate with thermal fluctuations to enhance local mobility. At low T , this effect tends to destabi-

lize crystalline order. Most importantly, fluctuations can also affect glassy dynamics in favor of a liquid one. As an example, the figure shows that for $R_c^2\rho = 0.8119$ and $T = 2.6$ [in units of $\hbar^2/(mR_c^2)$] the relaxation time sensibly decreases when the interaction strength is lowered from $mV_0/(\hbar^2 R_c^4) = 80$ to $mV_0/(\hbar^2 R_c^4) = 60$. These semiclassical results contrast those of Ref. [28] for a gas of polydispersed hard-sphere liquids, where increasing quantum fluctuations induces an increase of glassiness, and thus a re-entrant behavior, before melting. A discussion of this point will be presented elsewhere [48].

The effects of bosonic quantum statistics are shown in Fig. 4(b) using PIMC. There, we present results for the radial density-density correlation function defined as $g(r) = \langle \sum_j [\delta n / (2\pi r \delta r)] \rangle / N$, where δn is the number of particles at a distance between r and $r + \delta r$ from particle j . $g(r)$ is computed with Boltzmann particles (i.e., no particle exchanges, dashed line) as well as for Bose particles (i.e., including bosonic statistics, solid line) [49]. As an example, we choose $R_c^2\rho = 2.029$, $mV_0/(\hbar^2 R_c^4) = 35$, and $T/[\hbar^2/(mR_c^2)] = 10$. The figure shows that the density-density correlations in the semiclassical case are liquid-like. In particular, oscillations of $g(r)$ beyond the first correlation shell are strongly damped, and the value of $g(0)$ is approximately 2. However, this latter value increases by a factor of about 2 when quantum statistics is taken into account (solid line), i.e., in a fully quantum mechanical calculation. In addition, $g(r)$ displays more pronounced oscillations at finite r , signaling the enhancement of solid-like behavior. While less efficient for $R_c^2\rho < 1$, we find that this enhancement of solid-like properties is a general feature at sufficiently high density ($R_c^2\rho \gtrsim 1$) [50]. This is in contrast to the physics of non-cluster crystals, such as purely dipolar bosons [51, 52] or He^4 [2], as shown in Ref. [25].

In conclusion, we have demonstrated that a model of monodisperse cluster forming particles can realize a classical equilibrium phase which simultaneously breaks both translational symmetry and dynamic homogeneity. While the latter is usually associated with out-of-equilibrium glassy phenomena, here we find it at equilibrium. This results in the realization of a classical self-assembled cluster crystal with coexisting liquid-like properties, a direct analogy to quantum mechanical supersolid phases. In addition, we have illustrated a mechanism for glass formation in a monodisperse gas, where quantum mechanical fluctuations and statistics produce surprising competing effects. This work opens up exciting possibilities for observing soft-matter phenomena in the classical and quantum regimes in atomic physics. Of particular interest would be the study of other microscopic mechanisms for structural glass formation and the connection to spin glasses [27] in the quantum regime.

We thank T. Pohl for discussions. W. L. acknowledges support by the Austrian Science Fund through Grant No. P 25454-N27 and by the Institut fuer Quantenin-

formation. G. P. acknowledges support by the European Commission via ERC-St Grant ColdSIM (No. 307688), EOARD, and UdS via Labex NIE and IdEX, Initial Training Network COHERENCE, computing time at the HPC-UdS.

-
- [1] A. B. Kuklov, N. V. Prokofev, and B. V. Svistunov, *Physics* **4**, 109 (2011).
- [2] M. Boninsegni and N. V. Prokofev, *Rev. Mod. Phys.* **84**, 759 (2012).
- [3] M. H. W. Chan, R. B. Hallock, L. Reatto, *J. Low Temp. Phys.* **172**, (2013).
- [4] E. P. Gross, *Phys. Rev.* **106**, 161 (1957).
- [5] S. Saccani, S. Moroni, and M. Boninsegni *ibid.* **108**, 175301 (2012).
- [6] N. Henkel, R. Nath, and T. Pohl, *Phys. Rev. Lett.* **104**, 195302 (2010).
- [7] F. Cinti, P. Jain, M. Boninsegni, A. Micheli, P. Zoller and G. Pupillo, *Phys. Rev. Lett.* **105**, 135301 (2010).
- [8] F. Cinti, T. Macrì, W. Lechner, G. Pupillo and T. Pohl, *Nature Comm.* **5**, 3235 (2014).
- [9] I. Danshita and C. A. R. Sá de Melo, *Phys. Rev. Lett.* **103**, 225301 (2009); L. Pollet, J. D. Picon, H. P. Büchler, and M. Troyer, *ibid.* **104**, 125302 (2010); B. Capogrosso-Sansone, C. Trefzger, M. Lewenstein, P. Zoller, and G. Pupillo, *ibid.* **104**, 125301 (2010).
- [10] Y. Li, G. I. Martone, L. P. Pitaevskii, and S. Stringari, *Phys. Rev. Lett.* **110**, 235302 (2013).
- [11] M. Merolle, J. P. Garrahan, and D. Chandler, *PNAS* **102**, 10837-10840 (2005).
- [12] M. Scott Shell, P. G. Debenedetti, and F. H. Stillinger, *J. Phys: Condens. Matter.* **17**, S4025-S4046 (2005).
- [13] P. Charbonneau, A. Ikeda, G. Parisi and F. Zamponi, *PNAS* **109**, 35 13939 (2012).
- [14] K. Binder and W. Kob, *Glassy Materials and Disordered Solids*, World Scientific Publishing, London (2011).
- [15] P. G. Wolynes and V. Lubchenko, *Structural Glasses and Supercooled Liquids*, Wiley, New Jersey, (2012).
- [16] P. G. Debenedetti and F. H. Stillinger, *Nature* **410**, 259 (2001).
- [17] G. L. Hunter and E. R. Weeks, *Rep. Prog. Phys.* **75** 066501 (2012).
- [18] F. Sciortino, W. Kob and P. Tartaglia, *Phys. Rev. Lett.* **83**, 3214 (1999).
- [19] W. Götze, *J. Phys. Condens. Matter* **11**, A1 (1999).
- [20] H. Tanaka, T. Kawasaki, H. Shintani and K. Watanabe, *Nature Mat.* **9**, 324 (2010).
- [21] F. Sciortino and E. Zaccarelli, *Nature* **493**, 30-31 (2013).
- [22] F. Zamponi, *Nature Phys.* **7**, 99-100 (2011).
- [23] G. Biroli, C. Chamon, F. Zamponi, *Phys. Rev. B* **78**, 224306 (2008).
- [24] G. Carleo, M. Tarzia, and F. Zamponi, *Phys. Rev. Lett.* **103**, 215302 (2009).
- [25] M. Boninsegni, L. Pollet, N. Prokof'ev and B. Svistunov, *Phys. Rev. Lett.* **109**, 025302 (2012).
- [26] W. Lechner and P. Zoller, *Phys. Rev. Lett.* **111**, 185306 (2013).
- [27] I. Lesanovsky and J. P. Garrahan, *Phys. Rev. Lett.* **111**, 215305 (2013).
- [28] T. E. Markland, J. A. Morrone, B. J. Berne, K. Miyazaki, E. Rabani and D. R. Reichman, *Nature Phys.* **7**, 134 (2011).
- [29] A. Narros, A. J. Moreno, and C. N. Likos, *Soft Matter* **6**, 2435-2441 (2010).
- [30] Y. Li, Y. D. Tseng, S. Y. Kwon, L. d'Espaux, J. S. Bunch, P. L. McEuen, and D. Luo, *Nature Mater.* **3**, 38-42 (2004).
- [31] L. Santos, G. V. Shlyapnikov, P. Zoller and M. Lewenstein, *Phys. Rev. Lett.* **85**, 1791 (2000); G. Pupillo, A. Micheli, M. Boninsegni, I. Lesanovsky and P. Zoller, *Phys. Rev. Lett.* **104**, 223002 (2010); J. Honer, H. Weimer, T. Pfau and H. P. Büchler, *Phys. Rev. Lett.* **105**, 160404 (2010); J. B. Balewski, A. T. Krupp, A. Gaj, S. Hofferberth, R. Löw and T. Pfau, [arXiv:1312.6346](https://arxiv.org/abs/1312.6346).
- [32] N. Malossi, M.M. Valado, S. Scotti, P. Huillery, P. Pillet, D. Ciampini, E. Arimondo, and O. Morsch *Phys. Rev. Lett.* **113**, 023006 (2014); H. Schempp, G. Günter, M. Robert-de-Saint-Vincent, C. S. Hofmann, D. Breyel, A. Komnik, D. W. Schulte, M. Gärtner, J. Evers, S. Whitlock, M. Weidemüller, *ibid.* **112**, 013002 (2014); D. Barredo, S. Ravets, H. Labuhn, L. Béguin, A. Vernier, F. Nogrette, T. Lahaye, A. Browaeys, *ibid.* **112**, 183002 (2014); D. Maxwell, D. J. Szwer, D. Paredes-Barato, H. Busche, J. D. Pritchard, A. Gauguet, K. J. Weatherill, M. P. A. Jones and C. S. Adams, *ibid.* **110**, 103001 (2013); T. Baluksian, B. Huber, R. Löw and T. Pfau, *ibid.* **110**, 123001 (2013); M. Viteau, P. Huillery, M. G. Bason, N. Malossi, D. Ciampini, O. Morsch, E. Arimondo, D. Comparat, and P. Pillet, *ibid.* **109**, 053002 (2012); T. Peyronel, O. Firstenberg, Qi-Yu Liang, S. Hofferberth, A. V. Gorshkov, T. Pohl, M. D. Lukin and V. Vuletic, *Nature* **488**, 57 (2012); P. Schauß, M. Cheneau, M. Endres, T. Fukuhara, S. Hild, A. Omran, T. Pohl, C. Gross, S. Kuhr and I. Bloch, *Nature* **491**, 87 (2012).
- [33] Y. Pomeau and S. Rica, *Phys. Rev. Lett.* **72**, 2426 (1994).
- [34] F. Maucher *et al.*, *Phys. Rev. Lett.* **106**, 170401 (2011).
- [35] C. N. Likos, A. Lang, M. Watzlawek and H. Löwen, *Phys. Rev. E* **63**, 031206 (2001).
- [36] B. M. Mladek *et al.*, *Phys. Rev. Lett.* **96**, 045701 (2006).
- [37] D. Coslovich, L. Strauss and G. Kahl, *Soft Matter* **7**, 2127 (2011).
- [38] M. Montes-Saralegui, A. Nikoubashman and G. Kahl, *J. Phys.: Condens. Matter* **25**, 195101 (2013).
- [39] P. M. Chaikin and T. C. Lubensky. *Principles of Condensed Matter Physics*, Cambridge University Press, Cambridge, 1995.
- [40] We note that our definition of Φ_6 reduces to the standard definition of bond-order parameter for single-particle crystals, when $N_c = N$ (see, e.g., Ref. [41]). Technical details on the procedure we adopted to define a cluster are given in Ref. [42].
- [41] N. Gribova, A. Arnold, T. Schilling and C. Holm, *J. Chem. Phys.* **135**, 054514 (2011).
- [42] Supplemental Material
- [43] J-P. Hansen and I. R. McDonald, *Theory of Simple Liquids*, Academic Press (2013).
- [44] K. L. Ngai, *Relaxation and Diffusion in Complex Systems*, Springer, New York, 2011.
- [45] A. Widmer-Cooper, P. Harrowell and H. Fynewever, *Phys. Rev. Lett.* **93**, 135701 (2004).
- [46] M. Z. Slimani, P. Bacova, M. Bernabei, A. Narros, C. N. Likos and A. J. Moreno, [arXiv:1309.1061](https://arxiv.org/abs/1309.1061) (2014).
- [47] M. Boninsegni, N. Prokof'ev, and B. Svistunov *Phys. Rev. Lett.* **96**, 070601 (2006).
- [48] R. Díaz-Méndez *et al.*, in preparation.

- [49] Real-time dynamics is not directly accessible using quantum Monte-Carlo techniques, which are in turn exact for static observables, e.g. $g(r)$, in the presence of exchanges.
- [50] The solid-liquid phase transition becomes essentially density-independent for $R_c^2\rho \gg 1$, see F. Cinti, M. Boninsegni and T. Pohl, [arXiv:1402.0840](https://arxiv.org/abs/1402.0840) (submitted for publication).
- [51] H. P. Büchler et al., Phys. Rev. Lett. **98**, 060404 (2007).
- [52] G. E. Astrakharchik, J. Boronat, I. L. Kurbakov and Yu. E. Lozovik, Phys. Rev. Lett. **98**, 060405 (2007).

SUPPLEMENTARY MATERIAL

We introduce the algorithm used to identify the position of the clusters and the procedure to calculate the hexatic (short-range) order parameter Ψ_6 . The hopping mechanism at equilibrium is illustrated by sequential snapshots of a portion of the system. We shortly discuss the dynamic behavior of non-cluster-forming crystals with the example of purely repulsive particles in two dimensions.

CLUSTERING TECHNIQUE

In order to calculate the hexatic (short-range) order of the cluster crystal the first step is to distinguish between different clusters. We used a hierarchical clustering technique [1] that associates each particle to a single cluster in an unambiguous way.

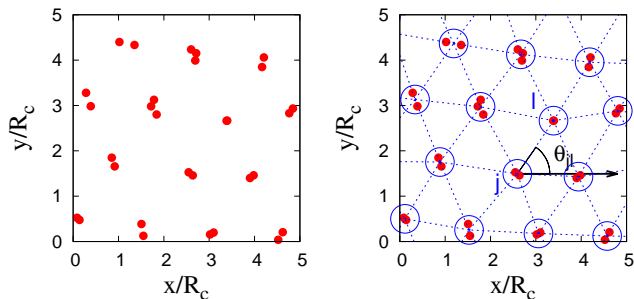


FIG. S1: Snapshot of a portion of the system in a cluster crystal configuration. Left panel: individual particles. Right panel: schematic outcome after the hierarchical clustering technique; blue circles are centered in cluster centroids, dashed blue segments connect nearest neighboring clusters, and θ_{jl} is the angle between the x axis and the line joining cluster j with its neighbor l .

For a given configuration of the system, the algorithm starts with $N_c = N$ one-particle clusters, corresponding to the N single particles and their positions. Then, an

iterative step consists in finding the minimum distance between all pair of clusters, in order to merge the two nearest clusters into a single one, and in relabeling the corresponding particles. The position of the new cluster (formed by the union of the previous two) is defined as the centroid of all the associated particles. The procedure ends when the minimum distance between pairs of clusters is greater than a fixed number d_c . In this way every step of the algorithm either decreases the number of clusters N_c in 1 or finishes.

The value of d_c has been set to $d_c = 0.7R_c$ in our calculations, roughly corresponding to half the value of the first peak in the density-density correlation function. This peak remains at the same position for all densities.

Hexatic order

Once the clusters are identified, the hexatic (short-range) order parameter of the cluster crystal can be calculated. The parameter is defined as

$$\Psi_6 = \left\langle \left| \frac{1}{N_c} \sum_j \frac{1}{N_j} \sum_l e^{i6\theta_{jl}} \right| \right\rangle \quad (2)$$

where N_j is the number of nearest neighbors of cluster j (see Fig. S1). We use the Voronoi construction in order to identify the nearest neighbors of each cluster. Angle θ_{jl} was always taken referred to the x axis.

HOPPING MECHANISM

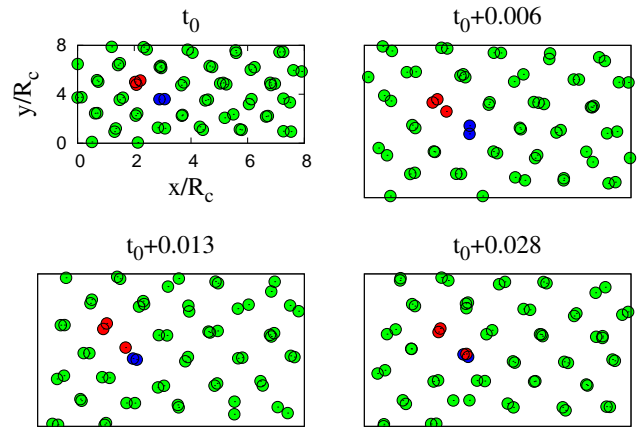


FIG. S2: Snapshots of the sequential evolution of a portion of the system, starting at $t = t_0$. Particles belonging to sites involved in a hopping process have been highlighted in colors red and blue.

The mechanism behind the slow relaxation of correlations in the solid phase corresponds to hopping of par-

ticles between different clusters. This hopping is an activated process, thus determining a relaxation time for the correlations, that diverges as the temperature is decreased to zero (see Fig. 2 in the main text).

For the case $R_c^2\rho > 1$ of interest here, this mechanism coexists with the hexatic bond-order of the clusters and the long range orientational order of the lattice. Figure S2 shows a series of snapshots of a small portion of the system in the hexatic bond-ordered phase in order to visualize the hopping mechanism.

DYNAMICS OF NON-CLUSTER FORMING CRYSTALS IN 2D

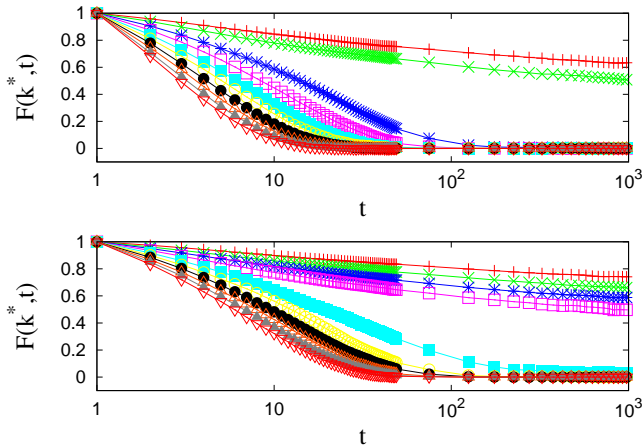


FIG. S3: Self intermediate scatter function for the soft core (upper panel) and completely repulsive (lower panel) potentials, for a density $R_c^2\rho = 0.487$ corresponding to no cluster (one particle per site) structure. In both panels temperatures are, from bottom to top: $T=0.025, 0.03, 0.035, \dots, 0.07$.

In this section we illustrate an example of the dynamic behavior of non-cluster forming crystals and compare it to the case of small densities $R_c^2\rho < 1$ for our model Eq. (1) in the main text, as a reference. The interesting case of intermediate densities $R_c^2\rho \lesssim 1$ will be the subject of a separate work [2].

Figure S3 (lower panel) shows the self-intermediate scatter function $F(k^*, t)$ (see main text for definition) as a function of t for a model system with purely repulsive interactions, corresponding to a regular non-cluster forming gas. We choose power-law interactions V_0/r^6 , in order to compare the results to those of our model in the low-density regime. The figure shows the expected behavior for regular (i.e., non-cluster-forming) liquids and crystals as a function of temperature T : by decreasing T the decay of $F(k^*, t)$ vs t is either essentially exponential (for high-enough T , corresponding to a liquid phase) or essentially constant (for low T , corresponding to a crystal phase).

For comparison, Fig. S3 (upper panel) shows an example for our model system [Eq. (1) in main text] and $R_c^2\rho \ll 1$, where soft-core interactions are dominated by the long-distance tail $1/r^6$, showing a decay similar to that of non-cluster-forming crystals, as expected. Both decays in Fig. S3 contrast with the two-step decay of Fig. 2 in the main text, typical of cluster-forming crystals.

-
- [1] P. Tan, M. Steinbach and V. Kumar, “Introduction to Data Mining”, Addison-Wesley, (2006).
 [2] R. Díaz-Méndez *et al.*, in preparation.